




Selection of antibody and light exposure regimens alters therapeutic effects of EGFR-targeted near-infrared photoimmunotherapy

Ryuhei Okada¹ · Takuya Kato¹ · Aki Furusawa¹ · Fuyuki Inagaki¹ · Hiroaki Wakiyama¹ · Daiki Fujimura¹ · Shuhei Okuyama¹ · Hideyuki Furumoto¹ · Hiroshi Fukushima¹ · Peter L. Choyke¹ · Hisataka Kobayashi¹ 

Received: 22 August 2021 / Accepted: 26 November 2021 / Published online: 11 January 2022
This is a U.S. government work and not under copyright protection in the U.S.; foreign copyright protection may apply 2021

Abstract

Near-infrared photoimmunotherapy (NIR-PIT) is a cell-specific cancer therapy that uses an antibody-photoabsorber (IRDye700DX, IR700) conjugate (APC) and NIR light. Intravenously injected APC binds the target cells, and subsequent NIR light exposure induces immunogenic cell death only in targeted cells. Panitumumab and cetuximab are antibodies that target human epidermal growth factor receptor (hEGFR) and are suitable for NIR-PIT. In athymic nude mouse models, panitumumab-based NIR-PIT showed superior therapeutic efficacy compared to cetuximab-based NIR-PIT because of the longer half-life of panitumumab-IR700 (pan-IR700) compared with cetuximab-IR700 (cet-IR700). Two light exposures on two consecutive days have also been shown to induce superior effects compared to a single light exposure in the athymic nude mouse model. However, the optimal regimen has not been assessed in immunocompetent mice. In this study, we compared panitumumab and cetuximab in APCs for NIR-PIT, and single and double light exposures using a newly established hEGFR-expressing cancer cell line derived from immunocompetent C57BL/6 mice (mEERL-hEGFR cell line). Fluorescence imaging showed that the decline of pan-IR700 was slower than cet-IR700 confirming a longer clearance time. Among all the combinations tested, mice receiving pan-IR700 and double light exposure showed the greatest tumor growth inhibition. This group was also shown to activate CD8⁺ T lymphocytes in lymph nodes and accumulate CD8⁺ T lymphocytes to a greater extent within the tumor compared with the control group. These results showed that APCs with longer half-life and double light exposure lead to superior outcomes in cancer cell-targeted NIR-PIT in an immunocompetent mouse model.

Keywords Photoimmunotherapy · mEERL · Panitumumab · Cetuximab · Epidermal growth factor receptor

Introduction

Near-infrared photoimmunotherapy (NIR-PIT) is a new cancer treatment that enables highly selective cancer cell destruction [1, 2]. Antibody-photoabsorber (IRDye700DX, IR700) conjugate (APC), which is intravenously injected, binds to the target molecule on the cancer cells within a day after APC administration. Subsequent NIR light exposure causes rapid cell death in APC-bound cells, which induces a necrotic/immunogenic cell death with minimal off-target effects [3–5]. Human epidermal growth factor receptor

(hEGFR) is commonly overexpressed in a wide variety of human cancers, including head and neck, breast, lung, colorectum, prostate, kidney, pancreas, brain, and bladder, and thus, is a good target for NIR-PIT [6]. A global phase-3 clinical trial in inoperable head and neck cancer is currently underway (<https://clinicaltrials.gov/ct2/show/NCT03769506>). In September 2020, the first APC for clinical use, cetuximab-IR700 conjugate (Akalux™, Rakuten Medical Inc.), and a NIR laser system (BioBlade™, Rakuten Medical Inc.) were approved for clinical use by the Pharmaceuticals and Medical Devices Agency (PMDA) in Japan.

Among the several parameters that might impact treatment efficacy of NIR-PIT is choice of antibody. Currently, three antibodies against hEGFR have been approved by the US Food and Drug Administration (FDA) for cancer treatment: cetuximab, panitumumab, and necitumumab. Among these three antibodies, cetuximab, a chimeric IgG1 antibody, and panitumumab, a fully humanized IgG2 antibody, have

✉ Hisataka Kobayashi
kobayash@mail.nih.gov

¹ Molecular Imaging Branch, Center for Cancer Research, National Cancer Institute, National Institutes of Health, Building 10, Room B3B69, MSC 1088, 10 Center Drive, Bethesda, MD 20892, USA

been widely used for more than 10 years [7]. These antibodies recognize similar epitopes on hEGFR and therefore compete with each other for binding to hEGFR, and they are remarkably similar to each other. However, panitumumab has a higher binding affinity and longer half-life in serum compared to cetuximab [8]. On the other hand, cetuximab has higher ADCC activity but also stronger potential immunogenicity than panitumumab due to its chimeric IgG1 subtype. In tumor-bearing athymic nude mice, panitumumab demonstrates a longer serum half-life which is considered desirable for NIR-PIT [9].

Another factor that affects the NIR-PIT therapeutic efficacy is the NIR light exposure schedule. While single light exposures one day after APC injection show efficacy, when a second light exposure is applied, there are enhanced therapeutic effects [10]. This is likely due to the temporarily increased permeability of the tumor vasculature following the first NIR-PIT treatment, which allows better microdistribution of the APC prior to the second light exposure [11]. NIR-PIT is a cell selective treatment that kills almost exclusively cancer cells but leaves other cells, including blood vessel endothelial cells, intact [12]. Selective destruction of perivascular cancer cells by NIR-PIT leads to immediate and dramatic increases in vascular permeability, resulting in an increase in APC delivery up to 24-fold compared with untreated tumors [13]. Unlike non-targeted small molecule photosensitizers, IR700-based APCs stay longer in the body after the initial light exposure and therefore could reaccumulate into the tumor to bind to the cancer cells, which allows the second light exposure to be highly effective [10]. Therefore, successful NIR-PIT favors longer-lived APCs in the circulation and double light doses.

Although the impact of antibody selection and number of light exposures on the efficacy of hEGFR-targeted NIR-PIT have been well studied in immunodeficient mice, there is little experience in immunocompetent mice because hEGFR-expressing tumor models in immunocompetent mice had not been available. The mEERL-hEGFR cell line is a newly developed murine cancer cell line derived from parental mEERL (mEERL-WT) cells [14]. mEERL-WT cells were made by transduction of human papillomavirus (HPV) E6/7 oncogenes and hRas to oropharyngeal epithelial cell from immunocompetent C57BL/6 mouse [15–17]. mEERL-hEGFR cells are further transduced with hEGFR. mEERL-hEGFR cells establish tumor when they are transplanted to C57BL/6 mice, and no host murine cells express hEGFR; therefore, mEERL-hEGFR is an ideal model simulating the clinical setting of hEGFR-targeted NIR-PIT to assess the therapeutic efficacy and immune reaction after therapy. Therefore, the aim of this study was to assess how the choice of antibody and number of light exposures could affect the therapeutic effects of hEGFR-targeted NIR-PIT in immunocompetent mice.

Materials and methods

Reagents

IR700 NHS ester was obtained from LI-COR Biosciences (Lincoln, NE, USA). Cetuximab was purchased from Bristol-Meyers Squibb (Princeton, NJ, USA). Panitumumab was purchased from Amgen (Thousand Oaks, CA, USA). All other chemicals were of reagent grade.

Synthesis of antibody–photoabsorber conjugate

Either cetuximab or panitumumab (1 mg) was incubated with fivefold molar excess of IR700 NHS ester in phosphate buffer (pH 8.5) at room temperature for 1 h. The mixture was purified with a Sephadex G25 column (PD-10; GE Healthcare, Piscataway, NJ, USA). IR700-conjugated cetuximab and panitumumab were referred to as cet-IR700 and pan-IR700, respectively. The quality of each conjugate was assessed with sodium dodecyl sulfate–polyacrylamide gel electrophoresis (SDS-PAGE) with a 4–20% gradient polyacrylamide gel (Life Technologies, Gaithersburg, MD, USA). Non-conjugated cetuximab and panitumumab were used for the controls. The APCs were also assessed with size exclusion chromatography (SEC) by the method previously described [18].

Cell culture

mEERL cells were established from oropharyngeal epithelial cells of C57BL/6 mouse by transduction of human papillomavirus E6/7 and hRAS [15–17]. mEERL-hEGFR cells were established by further transduction of hEGFR to parental mEERL cells (kind gift from Dr. William C. Spanos, Sanford Research, SD, USA) [14]. The cells were cultured by DMEM/F-12 (Thermo Fisher Scientific, Waltham, MA, USA) supplemented with 10% fetal bovine serum (Thermo Fisher Scientific), 100 U/mL penicillin and 100 µg/mL streptomycin (Thermo Fisher Scientific), and 1 × human keratinocyte growth supplement (Thermo Fisher Scientific) in a humidified incubator at 37 °C in an atmosphere of 95% air and 5% CO₂ [14].

Cell-specific binding analysis

Cetuximab or panitumumab was conjugated with Alexa Fluor 647 NHS Ester (Thermo Fisher Scientific). The conjugation was performed with the same method as that used in IR700 conjugation. Alexa647-conjugated cetuximab and panitumumab are abbreviated as cet-Alexa647 and pan-Alexa647, respectively. mEERL-hEGFR cells (5×10^5) were

incubated with 10 $\mu\text{g}/\text{mL}$ of cet-Alexa647 or pan-Alexa647 for 1 h at 37 °C. After washing with PBS, the cells were stained with Fixable Viability Dye (Thermo Fisher Scientific) for 30 min at 4 °C. To confirm the specific binding of the Alexa 647-conjugated antibodies, onefold, tenfold, or 100-fold molar excess of either cetuximab or panitumumab was added to some samples 1 h prior to the administration of the cet-Alexa647 or pan-Alexa647. The cells were then analyzed with FACSLyric (BD Biosciences) and FlowJo software (BD Biosciences).

In vitro NIR-PIT

mEERL-hEGFR cells (2×10^5) were seeded into each corner well of 12-well plate. After one day, the cells were incubated with 10 $\mu\text{g}/\text{mL}$ of each APC for 1 h at 37 °C. After washing with PBS, the cells were exposed to NIR light (690 nm, 100 mW/cm^2) at 0, 15, or 30 J/cm^2 using an ML7710 laser system (Modulight, Tampere, Finland). After 1 h, the cells were collected with trypsin and stained with 1 $\mu\text{g}/\text{mL}$ propidium iodide (PI). PI-stained cell percentage was analyzed with a flow cytometer (FACSCalibur, BD Biosciences) and FlowJo software (BD Biosciences).

Animals and tumor models

All in vivo procedures were conducted in compliance with the Guide for the Care and Use of Laboratory Animal Resources (1996), US National Research Council, and approved by the local Animal Care and Use Committee. All in vivo procedures were performed under anesthesia by inhalation of 2–4% isoflurane and/or intraperitoneal injection of 0.75 mg of sodium pentobarbital (Ovation Pharmaceuticals, Deerfield, IL, USA). Six- to eight-week-old female C57BL/6 mice were purchased from The Jackson Laboratory (Bar Harbor, ME, USA). mEERL-hEGFR cells (2×10^6) were inoculated into the right dorsum of the mice. The hair on the tumor area was removed for NIR light exposure and fluorescence imaging studies. Tumor volume was calculated as (major axis) \times (minor axis)² \times 0.5, based on caliper measurement. Tumor volume was measured twice a week until the volume reached the endpoint (1000 mm^3), whereupon the mice were euthanized with CO_2 .

In vivo fluorescence imaging

Each APC (100 μg) was injected via lateral tail vein 6 days after tumor transplantation. Serial dorsal and ventral fluorescence images were obtained with the 700-nm fluorescence channel of a Pearl Imager (LI-COR Bioscience). The images were taken before and 1, 3, 6, 9, 12, 24, 48, 72, and 96 h after APC administration. The images were analyzed with Pearl Cam Software (LI-COR Bioscience). Regions of

interest (ROIs) were drawn on the tumor/liver and the non-tumor/liver region (background) on the same picture. Target-to-background ratio was calculated as (mean fluorescence intensity of the target)/(mean fluorescence intensity of the background).

In vivo NIR-PIT

mEERL-hEGFR cells (2×10^6) were inoculated on day 0. Tumor-bearing mice were randomized into five experimental groups as follows: (1) no treatment (control), (2) intravenous administration of cet-IR700 (100 μg) followed by single-NIR light exposure (cet-single-NIR), (3) intravenous administration of cet-IR700 (100 μg) followed by double-NIR light exposure (cet-double-NIR), (4) intravenous administration of pan-IR700 (100 μg) followed by single-NIR light exposure (pan-single-NIR), and (5) intravenous administration of pan-IR700 (100 μg) followed by double-NIR light exposure (pan-double-NIR). The APCs were injected on day 6, and NIR light exposure (690 nm, 100 mW/cm^2 , 30 J/cm^2) was performed either only on day 7 (single exposure) or day 7 and 8 (double exposure). Tumor fluorescence intensity of IR700 was assessed before and after each light exposure as described above.

Flow cytometry analysis of tumor-draining lymph nodes

Tumor-draining lymph nodes were extracted two days after the initial light exposure (i.e., day 9), and single cell suspension was prepared with mechanical crushing and filtration (70 μm). The cells were stained with anti-CD45 (clone 30-F11, Thermo Fisher Scientific), anti-CD3 ϵ (clone 145-2C11, BioLegend, San Diego, CA, USA), anti-CD8 α (clone 53–6.7, Thermo Fisher Scientific), anti-CD25 (clone PC61, BioLegend), and anti-CD69 (clone H1.2F3, Thermo Fisher Scientific). To exclude the dead cells from the study, the cells were also stained with Fixable Viability Dye (Thermo Fisher Scientific). The cells were then analyzed with FACSLyric (BD Biosciences) and FlowJo software (BD Biosciences).

Multicolor immunofluorescence staining

Multicolor immunofluorescence staining was performed to analyze the tumor-infiltrating lymphocytes using Opal 7-color Automation IHC Kit (Akoya Bioscience, Menlo Park, CA, USA) and Bond RXm auto stainer (Leica Biosystems, Wetzlar, Germany) according to the protocol previously described [18]. Three pictures were taken for each

specimen, and each parameter was summed. Cell density was calculated as cell counts per square millimeter.

Statistical analysis

Data are expressed as means \pm SEM. Statistical analysis was performed with GraphPad Prism (GraphPad Software, La Jolla, CA, USA). For the assessment of the cytotoxicity of in vitro NIR-PIT, flow cytometry of the lymph nodes, and immunohistochemical staining study, a one-way ANOVA followed by Tukey's test was used. For comparison of quantitative fluorescence intensity and tumor volume, a repeated-measures two-way ANOVA followed by Sidak's test (two groups) or Tukey's test (three or more groups) was used. The cumulative probability of survival based on tumor volume (1000 mm³) was estimated with the Kaplan–Meier survival curve analysis, and the results were compared with log-rank test with Bonferroni correction. *P*-value of less than 0.05 was considered significant.

Results

IR700 was successfully conjugated with both antibodies

IR700 was conjugated with either cetuximab (cet-IR700) or panitumumab (pan-IR700). Conjugated APCs were analyzed with SDS-PAGE (Fig. 1A). Each APC showed similar molecular weight to its unconjugated counterpart antibody, but only APCs showed 700-nm fluorescence. Quality of APC was also assessed with SEC (Fig. 1B). In both APCs, the majority of the protein, which was shown as a peak at 280 nm, showed absorption of 689 nm. These results verified the successful conjugation of both panitumumab and cetuximab APCs.

NIR-PIT with both antibodies showed similar in vitro cytotoxicity

To verify the in vitro binding of the two antibodies to mEERL-hEGFR cells, the cells were incubated with Alexa 647-conjugated antibodies (cet-Alexa647 and pan-Alexa647). Both antibodies showed fluorescence shift compared with unstained samples consistent with binding (Fig. 1C). To compare the affinities of the two antibodies, unconjugated cetuximab or panitumumab (onefold, tenfold, or 100-fold molar excess) was added to some samples prior to the incubation with Alexa 647-conjugated antibodies. Although both unconjugated antibodies attenuated the fluorescence signal in a concentration-dependent manner, panitumumab blocked the signal more effectively than cetuximab. These results suggested that both antibodies

specifically bind to mEERL-hEGFR cells but that the affinity of panitumumab is higher than cetuximab. In vitro binding of IR700 conjugated APCs (cet-IR700 and pan-IR700) to the cells was also assessed. The cells were incubated with each APC, and flow cytometry was performed (Fig. S1). In both APCs, fluorescence shift was seen after incubation with the cells, and these shifts were completely attenuated by adding excess unconjugated antibodies, verifying the specific binding of the two APCs to mEERL-hEGFR cells. In vitro cytotoxicity of NIR-PIT performed with each APC was quantitatively compared by flow cytometry (Fig. 1D). mEERL-hEGFR cells were incubated with each APC then exposed to NIR light. With both APCs, the dead cell percentage was increased in a light dose-dependent manner. No increase in cell death was shown after administration of the APC alone or NIR light exposure alone. No significant difference was seen between the two APCs at the same light dose. These results verified that the in vitro cytotoxicity of both APCs following NIR-PIT was the same.

Cet-IR700 was cleared faster than pan-IR700 in the murine model

To compare the biodistribution and clearance, both APCs were intravenously injected and serial 700-nm fluorescence images were obtained. With both APCs, the fluorescence in the tumor and liver, which are the signs of tumor accumulation and hepatic clearance of APC, respectively, were clearly detected within one hour of APC injection (Fig. 2A). A 700-nm fluorescence in the tumor and liver was quantitatively compared for injections of cet-IR700 and pan-IR700 (Fig. 2B). The peak average fluorescence intensities of cet-IR700 and pan-IR700 were shown at 9 and 12 h after the APC administration, respectively. The fluorescence gradually decreased over the following days in both APCs. The average peak fluorescence of tumor was significantly higher in pan-IR700 than cet-IR700 at 12 and 24 h after the injection. Meanwhile, the average peak fluorescence intensity of the liver was significantly higher in the cet-IR700 than in pan-IR700 in early phase. These results suggested the faster clearance of cet-IR700 compared with pan-IR700.

Double light exposure showed superior NIR-PIT effect to single light exposure

To assess the impact of antibody selection for each APC and light exposure times (one vs. two exposures of light per APC injection) on the efficacy of in vivo NIR-PIT, mEERL-hEGFR cells were inoculated into the right dorsum of C57BL/6 mice. Tumor-bearing mice were randomized into the following five experimental groups: no treatment (control), cet-IR700 injection and single-NIR light exposure (cet-single-NIR), cet-IR700 injection and

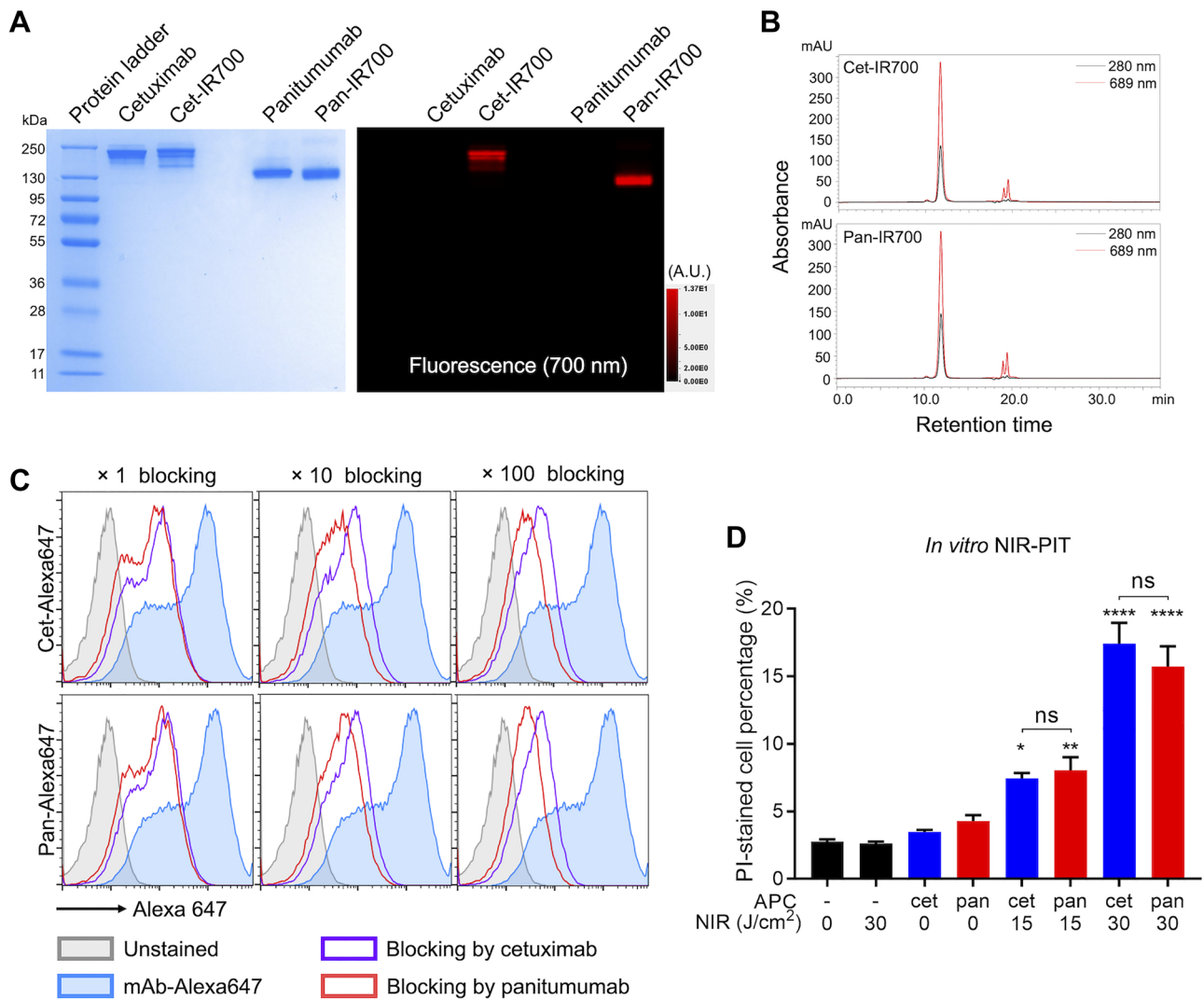


Fig. 1 In vitro NIR-PIT **A**, Both APCs were assessed with SDS-PAGE. Left, Colloidal blue; right, 700-nm fluorescence. A.U., arbitrary unit. **B**, The APCs were assessed with SEC. Absorbances of 280 and 689 nm were measured. **C**, Flow cytometry analysis of the antibody affinity to the mEERL-hEGFR cells. Alexa 647-conjugated antibody was incubated with the cells. The fluorescence signals were

blocked with either unconjugated antibody of 1, 10, or 100 molar excess. **D**, Quantitative cell viability assay after each therapy. The dead cell percentage was assessed with propidium iodide (PI) staining by flow cytometry ($n=4$; one-way ANOVA followed by Tukey's test; *, $p < 0.05$; **, $p < 0.01$; ****, $p < 0.0001$ vs. untreated samples; ns, not significant between two groups)

double-NIR light exposure (cet-double-NIR), pan-IR700 injection and single-NIR light exposure (pan-single-NIR), and pan-IR700 injection and double-NIR light exposure (pan-double-NIR). The treatment regimen and fluorescence imaging schedule are shown in Fig. 3A. mEERL-hEGFR cancer cells were inoculated on the right dorsum (day 0), and NIR light was applied one day after APC injection. Only the tumor region was exposed to NIR light, and other areas were shielded with aluminum foil during the light irradiation (Fig. 3B). The 700-nm fluorescence images were obtained before and after each light exposure (Fig. 3C). The fluorescence intensity was quantitatively

compared among the five groups (Fig. 3D). On the first light exposure day (day 7), all mice in the four NIR-PIT treated groups received light exposure. The average fluorescence intensity of the tumors significantly decreased after the light exposure compared to baseline in all groups irradiated with NIR light. The average fluorescence intensity of tumor site increased between the first exposure until just before the second light exposure (day 8) in all the treated groups. After the second NIR light exposure (i.e., cet-double-NIR group and pan-double-NIR group), the fluorescence of tumor was significantly attenuated, whereas no significant change of the tumor fluorescence

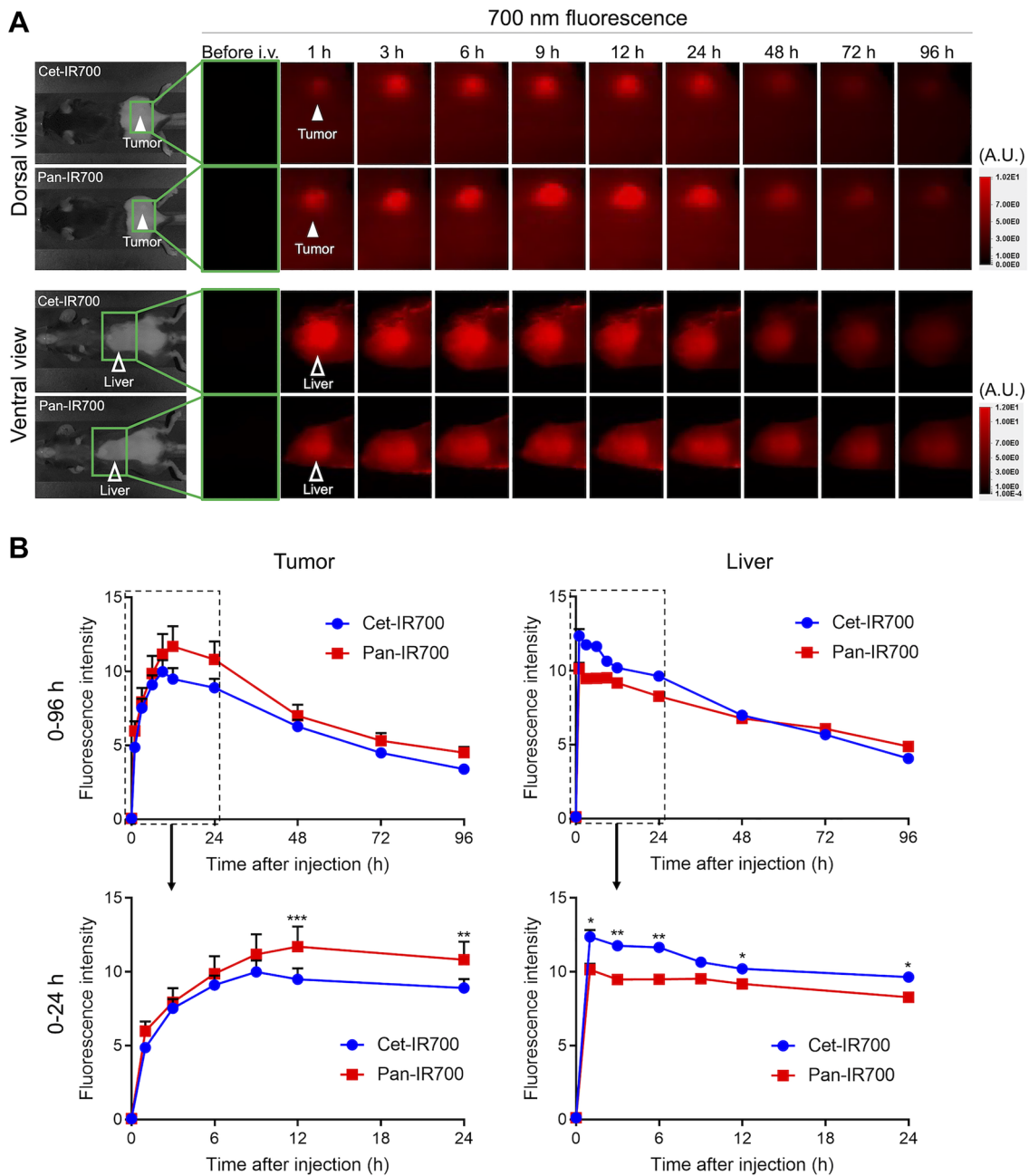


Fig. 2 Fluorescence imaging study **A**, Serial 700-nm fluorescence images were obtained after intravenous injection of each APC. Tumor and liver were assessed with dorsal and ventral views, respectively. Filled arrowhead, tumor; open arrowhead, liver. A.U., arbitrary unit. **B**, Mean fluorescence intensity was compared between two APCs.

Upper, graphs of all time points (0–96 h after the injection); lower, magnified graph of the early phase (0–24 h after the injection) ($n=7$; repeated-measures two-way ANOVA followed by Sidak's test; *, $p<0.05$; **, $p<0.01$; ***, $p<0.001$)

was observed in single-NIR groups. The fluorescence intensity was compared between the cet-IR700-based NIR-PIT groups (cet-single-NIR group + cet-double-NIR group) and the pan-IR700 groups (pan-single-NIR group + pan-double-NIR group) prior to each light exposure (Fig. 3E). On both days, pan-IR700 groups showed

significantly higher fluorescence in the tumor than the cet-IR700 groups.

The therapeutic efficacy was compared based on changes in tumor volume (Fig. 3F). All treatment groups significantly suppressed tumor growth compared with the control group. No significant difference was observed between the cet-single-NIR group and pan-single-NIR group. The

pan-double-NIR group suppressed tumor growth significantly more than other treatment groups. Although the cet-double-NIR group showed a slightly greater tumor volume reduction compared with the single-NIR groups, the difference was small and not statistically significant. On the other hand, the pan-double-NIR group experienced significantly prolonged survival compared with the control group (Fig. 3G). No other significant differences were observed between any other two groups.

Cytotoxic T lymphocytes in the regional lymph nodes were activated after NIR-PIT

To assess T cell activation within the tumor-draining lymph nodes after each therapy, inguinal lymph nodes were extracted two days after the initial light exposure (i.e., on day 9) and analyzed with flow cytometry. Early T cell activation markers on CD8⁺ T cells were compared among the five groups (Fig. 4). All the treated groups showed a significantly higher percentage of CD69- or CD25-positive cells among CD8⁺ T cells compared with the control group. Although the double-NIR groups showed a trend of higher CD25-positive cells compared with the corresponding single-NIR groups, the difference was not significant.

Intratumoral CD8⁺ T cells were increased in pan-double-NIR group after therapy

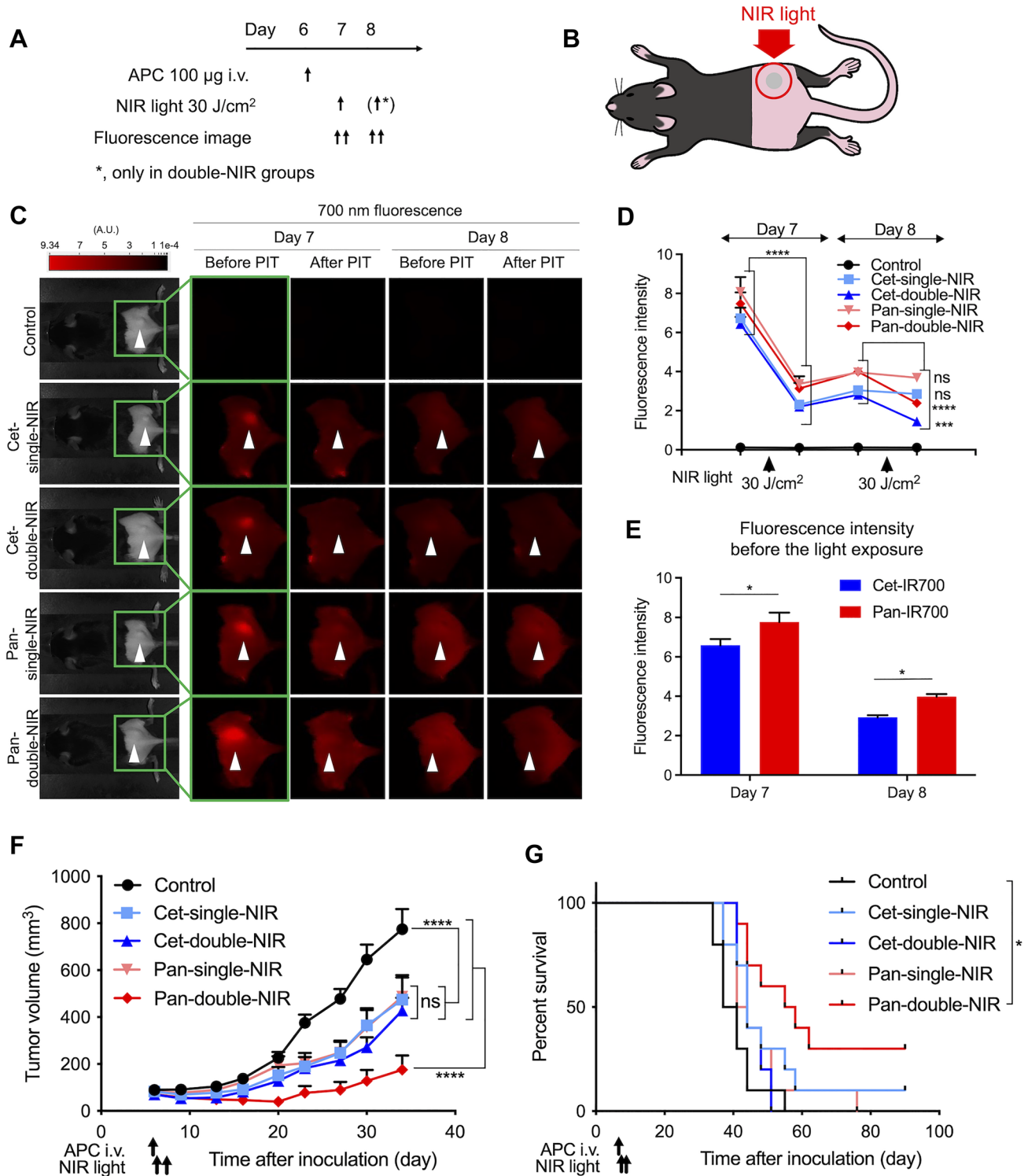
To compare the tumor microenvironment (TME) after each therapy, tumors were extracted 7 days after the initial light exposure (i.e., on day 14) and analyzed with multiplex immunohistochemical staining (IHC) (Fig. 5). Intratumoral lymphocytes were quantitatively analyzed. Pan-double-NIR group showed significantly increased intratumoral CD8⁺ T cell density compared with the control group. No significant difference was seen among other groups. For CD4⁺Foxp3⁻ helper T cell and CD4⁺Foxp3⁺ regulatory T cell (Treg), no significant differences were seen among groups (Fig. S2).

Discussion

We compared two anti-hEGFR antibodies, cetuximab and panitumumab, and two different light exposure schedules to optimize NIR-PIT efficacy. The results demonstrated that panitumumab-based NIR-PIT with double light exposure induces the strongest antitumor effect. The longer half-life and stronger binding of the panitumumab APC were thought to provide an advantage in NIR-PIT especially with multiple light exposures. The pharmacokinetic fluorescent imaging of APC-injected mice suggested faster clearance of cet-IR700 compared with pan-IR700 from C57BL/6 immunocompetent

mice despite the fact that cetuximab is a chimeric IgG1 antibody, a part of which was derived from mice while panitumumab is a fully human IgG2 antibody [19], which would be expected to be cleared from the mouse faster. The results in immunocompetent mice were consistent with the results in athymic nude mice [9]. In the NIR-PIT in vivo experiment, although tumor fluorescence intensity was significantly higher with pan-IR700 than with cet-IR700 prior to the first NIR light exposure, the therapeutic effects were comparable when there was only one light exposure (Fig. 3E and 3F). These results suggest that sufficient APC accumulated within the tumors to make NIR-PIT effective irrespective of the different clearance rates at 24 h. However, when a second light exposure was added a day later the pan-double-NIR group showed greater tumor suppression than the single light exposure groups, while cet-double-NIR group showed no significant difference compared with single light exposure groups. These differences of therapeutic efficacy are likely due to the longer clearance time of the panitumumab APC, the differences becoming more obvious at 48 h post-injection. The fluorescence of the tumor region was significantly higher with pan-IR700 one day after the initial light exposure, i.e., just before the second light exposure. In the cet-double-NIR group, circulating APC after the initial light exposure decreased faster; therefore, there was less residual APC to reaccumulate in the tumor. This reduced the effect of the second light exposure. Another possible factor affecting the therapeutic efficacy is antibody binding affinity. In vitro binding to mEERL-hEGFR cells was stronger with panitumumab than cetuximab (Fig. 1C), corresponding to higher panitumumab affinity (about eightfold greater) to hEGFR compared to cetuximab [8]. Notwithstanding this higher affinity, in vitro NIR-PIT showed comparable cytotoxicity between cet-IR700 and pan-IR700 (Fig. 1D). Moreover, in vivo NIR-PIT with a single light exposure (cet-single-NIR and pan-single-NIR) resulted in comparable tumor growth suppression (Fig. 3F), suggesting binding affinity is not a critical determinant of therapeutic efficacy, at least in this tumor model. Even though the binding affinity might affect clearance, we concluded that clearance of the APC itself is the most important factor in determining effectiveness, especially for double light exposure NIR-PIT.

The use of immunocompetent mice in this study allowed study of immune reactions induced after hEGFR-targeted NIR-PIT. T cell activation markers were investigated in the tumor-draining lymph nodes two days after the initial light exposure (Fig. 4). CD69 or CD25 positive rate among CD8⁺ T cells was significantly higher in all the treated groups compared with controls. It is notable that these positive rates showed no significant difference among the four treated groups. Although some differences might be detected at other timepoint, these results suggest that cancer cell-targeted NIR-PIT activates host antitumor immunity even



after a single light exposure. In multiplex IHC, although the average intratumoral CD8^+ T cell density was higher in all treated groups, only the pan-double-NIR group showed statistically significant higher densities (Fig. 5). Even though this may be because the pan-double-NIR therapy killed more cancer cells, increased CD8^+ T cell density might lead to

greater tumor growth suppression and better therapeutic outcome. The pan-double-NIR group showed the highest rate of complete response among the treated groups, which is likely the result of upregulated host immunity. Tumor destruction on two consecutive days may result in not only more cancer cell reduction but also superior host immune activation.

Fig. 3 In vivo NIR-PIT **A**, treatment and imaging schedule. In cet-single-NIR and pan-single-NIR groups, NIR light was applied only once on one day after the APC injection, while in cet-double-NIR and pan-double-NIR groups, the light was applied on the following two days after the APC injection. A.U., arbitrary unit. **B**, Diagram of NIR light exposure. Tumor was established on the right dorsum, and NIR light was applied only to the tumor; all other parts of the body were covered with aluminum foil during the light exposure. **C**, Fluorescence images were obtained before and after the light exposure on the two days on which NIR light was applied. Arrowheads represent the location of tumors. **D**, Quantitative analysis of the fluorescence intensity of tumor region. ($n=10$; repeated-measures two-way ANOVA followed by Tukey’s test; ***, $p<0.001$; ****, $p<0.0001$, ns; not significant; vs. before each NIR light application). **E**, Tumor fluorescence intensity before the light exposure was compared between cet-IR700 groups (cet-single-NIR and cet-double-NIR) and pan-IR700 groups (pan-single-NIR and pan-double-NIR) groups on each treatment day ($n=20$; two-way ANOVA followed by Sidak’s test; *, $p<0.05$). **F**, Tumor volume curves ($n=10$; repeated measures two-way ANOVA followed by Tukey’s test; ****, $p<0.0001$, ns, not significant). **G**, Survival curves based on the tumor volume (end-point, 1,000 mm³) ($n=10$; log-rank test with Bonferroni correction; *, $p<0.05$)

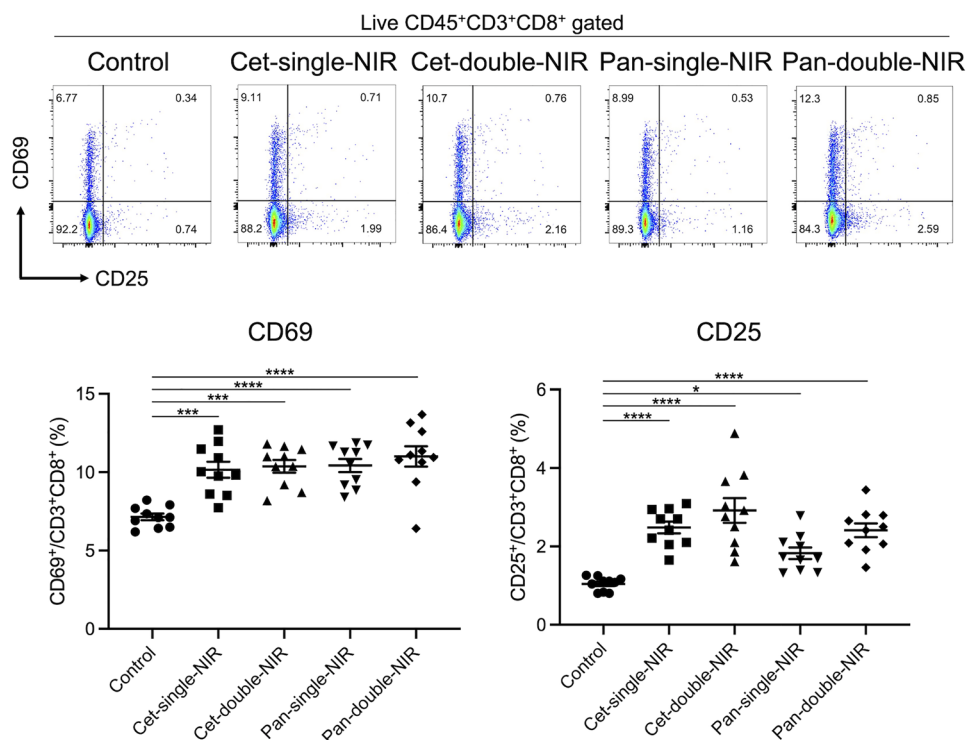
NIR-PIT can be applied to many other types of cells including intratumoral immune suppressive cells, examples of which include Tregs, which are present in the mEERL-hEGFR tumor. Tregs play a major immunosuppressive role in the tumor microenvironment and could be depleted with CD25- or CTLA4-targeted NIR-PIT [18, 20, 21]. The combination of Treg-targeted NIR-PIT and pan-double-NIR-PIT might improve treatment efficacy in EGFR-positive tumors with a Treg infiltration [14, 22]. However,

the treatment schedule should be carefully considered because activated T cells also express CD25 and CTLA4, so the second NIR light exposure could end up simply damaging T cells newly activated after the first NIR light exposure, thus working at cross purposes with the intent of the therapy.

Although this tumor model improves upon the immunocompetent models used before, there are still several limitations to this study. First, we used only one cell line largely because we tailor-made this unique hEGFR-expressing murine cancer model for clinically approved cet-IR700 in order to be able to test NIR-PIT in rodents. Second, we used a subcutaneous tumor model. Orthotopic tumor models would be superior for reflecting tumor microenvironment [23, 24]. Third, we used fixed APC dose of 100 µg for both APCs. Cetuximab-based NIR-PIT with double light exposure may show superior efficacy with larger amounts of cet-IR700. However, we fixed the APC dose because we aimed to elucidate the impact of clearance in the current study. Fourth, the pharmacokinetics of cet-IR700 and pan-IR700 in humans might be different from mice. Therefore, the results may differ in clinical human use. According to the prescribing information, the half-lives of cetuximab and panitumumab are 4.6 days (range 2.6–9.5 days) and 7.5 days (range 3.6–10.6 days), respectively, in general agreement with the results of this study. As conjugation to IR700 could lead to the shorter half-life of the antibody, further pharmacokinetic studies are needed for clinical translation.

Thus, this is the first report that compares the therapeutic efficacy of NIR-PIT using two different antibodies targeting

Fig. 4 CD8⁺ T cell activation within tumor-draining lymph nodes CD8⁺ T cells within tumor-draining lymph nodes were assessed with flow cytometry two days after the initial light exposure. Expression of early-phase T cell activation markers, CD69 and CD25, were analyzed. Scatter plots show representative results of CD69 and CD25 expression among live CD8⁺ T cells. Dot plots show the CD69- and CD25-positive percentages among CD8⁺ T cells ($n=10$; one-way ANOVA followed by Tukey’s test; *, $p<0.05$; ***, $p<0.001$; ****, $p<0.0001$)



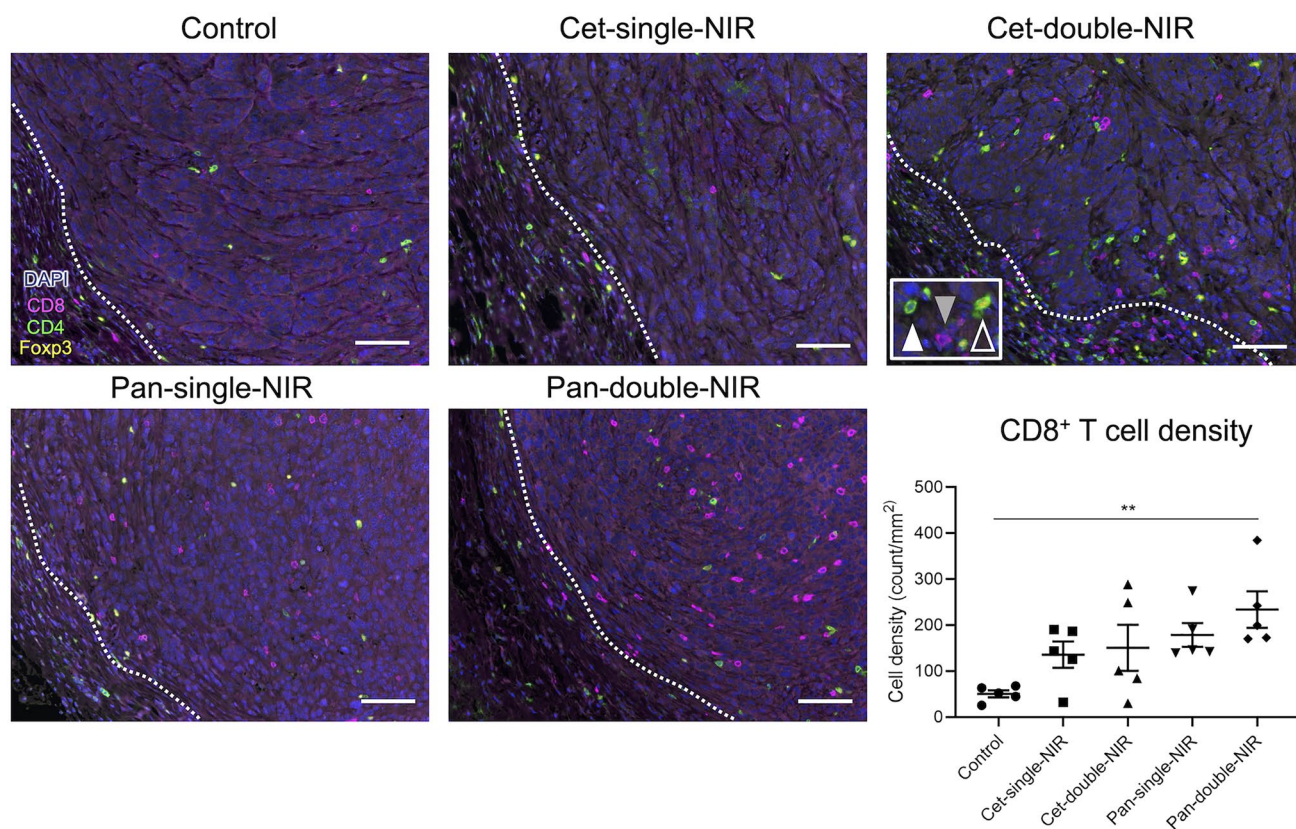


Fig. 5 CD8⁺ T cell accumulation into tumor 7 days after the initial light exposure. The specimens were assessed by multiplex IHC staining with anti-CD8 (magenta), anti-CD4 (green), anti-Foxp3 (yellow), and DAPI (blue). Photos show representative results of each treatment group. CD8⁺ cell (gray-filled arrowhead), CD4⁺Foxp3⁻ cell

(white-filled arrowhead), and CD4⁺Foxp3⁺ cell (white open arrowhead) were counted. White dotted lines indicate tumor edges. Scale bar=100 μ m. Dot plots show the intratumoral CD8⁺ cell density in each experimental group ($n=5$; one-way ANOVA followed by Tukey's test; **, $p < 0.01$)

hEGFR in immunocompetent mice. Clearance rates appear to be a defining feature of APC for the efficacy of NIR-PIT, with longer half-lived APCs having the advantage. Slower clearance APCs not only improve tumor killing but also induce stronger immune reactions. Antibodies with longer half-life and double light exposure are thought to induce greater efficacy in cancer cell-targeted NIR-PIT.

Supplementary Information The online version contains supplementary material available at <https://doi.org/10.1007/s00262-021-03124-x>.

Authors' contributions R.O. mainly designed and conducted experiments, performed analysis and wrote the manuscript; T.K., A.F., F.I., H.W., D.F., S.O., H.F., and H.F. performed experiments and analysis; P.L.C. wrote the manuscript and supervised the project; and H.K. planned and initiated the project, designed and conducted experiments, wrote the manuscript, and supervised the entire project.

Funding This research was supported by the Intramural Research Program of the National Institutes of Health, National Cancer Institute, Center for Cancer Research (ZIA BC011513). F.I. was also supported with a grant from National Center for Global Health and Medicine Research Institute, Tokyo, Japan.

Declarations

Conflict of interest The authors have no conflict of interest to disclose.

Ethics approval Animal studies were approved by the local Animal Care and Use Committee (MIP-003; project number P183735).

References

1. Kobayashi H, Choyke PL (2019) Near-infrared photoimmunotherapy of cancer. *Acc Chem Res* 52:2332–2339. <https://doi.org/10.1021/acs.accounts.9b00273>
2. Kobayashi H, Griffiths GL, Choyke PL (2020) Near-Infrared Photoimmunotherapy: photoactivatable antibody-drug conjugates (ADCs). *Bioconjug Chem* 31:28–36. <https://doi.org/10.1021/acs.bioconjchem.9b00546>
3. Mitsunaga M, Ogawa M, Kosaka N, Rosenblum LT, Choyke PL, Kobayashi H (2011) Cancer cell-selective in vivo near infrared

- photoimmunotherapy targeting specific membrane molecules. *Nat Med* 17:1685–1691. <https://doi.org/10.1038/nm.2554>
4. Ogawa M, Tomita Y, Nakamura Y et al (2017) Immunogenic cancer cell death selectively induced by near infrared photoimmunotherapy initiates host tumor immunity. *Oncotarget* 8:10425–10436. <https://doi.org/10.18632/oncotarget.14425>
 5. Sato K, Ando K, Okuyama S et al (2018) Photoinduced ligand release from a silicon phthalocyanine dye conjugated with monoclonal antibodies: a mechanism of cancer cell cytotoxicity after near-infrared photoimmunotherapy. *ACS Cent Sci* 4:1559–1569. <https://doi.org/10.1021/acscentsci.8b00565>
 6. Martinelli E, De Palma R, Orditura M, De Vita F, Ciardiello F (2009) Anti-epidermal growth factor receptor monoclonal antibodies in cancer therapy. *Clin Exp Immunol* 158:1–9. <https://doi.org/10.1111/j.1365-2249.2009.03992.x>
 7. Tebbutt N, Pedersen MW, Johns TG (2013) Targeting the ERBB family in cancer: couples therapy. *Nat Rev Cancer* 13:663–673. <https://doi.org/10.1038/nrc3559>
 8. Kim GP, Grothey A (2008) Targeting colorectal cancer with human anti-EGFR monoclonal antibodies: focus on panitumumab. *Biologics* 2:223–228. <https://doi.org/10.2147/btt.s1980>
 9. Sato K, Watanabe R, Hanaoka H, Harada T, Nakajima T, Kim I, Paik CH, Choyke PL, Kobayashi H (2014) Photoimmunotherapy: comparative effectiveness of two monoclonal antibodies targeting the epidermal growth factor receptor. *Mol Oncol* 8:620–632. <https://doi.org/10.1016/j.molonc.2014.01.006>
 10. Mitsunaga M, Nakajima T, Sano K, Choyke PL, Kobayashi H (2012) Near-infrared theranostic photoimmunotherapy (PIT): repeated exposure of light enhances the effect of immunocjugate. *Bioconjug Chem* 23:604–609. <https://doi.org/10.1021/bc200648m>
 11. Nakamura Y, Mochida A, Choyke PL, Kobayashi H (2016) Nanodrug delivery: is the enhanced permeability and retention effect sufficient for curing cancer? *Bioconjug Chem* 27:2225–2238. <https://doi.org/10.1021/acs.bioconjchem.6b00437>
 12. Wu S, Okada R, Liu Y et al (2021) Quantitative analysis of vascular changes during photoimmunotherapy using speckle variance optical coherence tomography (SV-OCT). *Biomed Opt Express* 12:1804–1820. <https://doi.org/10.1364/boe.419163>
 13. Sano K, Nakajima T, Choyke PL, Kobayashi H (2013) Markedly enhanced permeability and retention effects induced by photoimmunotherapy of tumors. *ACS Nano* 7:717–724. <https://doi.org/10.1021/nn305011p>
 14. Okada R, Furusawa A, Vermeer DW et al (2021) Near-infrared photoimmunotherapy targeting human-EGFR in a mouse tumor model simulating current and future clinical trials. *EBioMedicine* 67:103345. <https://doi.org/10.1016/j.ebiom.2021.103345>
 15. Hoover AC, Spanos WC, Harris GF, Anderson ME, Klingelhut AJ, Lee JH (2007) The role of human papillomavirus 16 E6 in anchorage-independent and invasive growth of mouse tonsil epithelium. *Archives of otolaryngology–Head & Neck Surgery*. 133: 495–502. doi: <https://doi.org/10.1001/archotol.133.5.495>
 16. Spanos WC, Hoover A, Harris GF et al (2008) The PDZ binding motif of human papillomavirus type 16 E6 induces PTPN13 loss, which allows anchorage-independent growth and synergizes with ras for invasive growth. *J Virol* 82:2493–2500. <https://doi.org/10.1128/jvi.02188-07>
 17. Williams R, Lee DW, Elzey BD, Anderson ME, Hostager BS, Lee JH (2009) Preclinical models of HPV+ and HPV- HNSCC in mice: an immune clearance of HPV+ HNSCC. *Head Neck* 31:911–918. <https://doi.org/10.1002/hed.21040>
 18. Okada R, Kato T, Furusawa A, Inagaki F, Wakiyama H, Choyke PL, Kobayashi H (2021) Local depletion of immune checkpoint ligand CTLA4 expressing cells in tumor beds enhances antitumor host immunity. *Adv Ther (Weinh)*. <https://doi.org/10.1002/adtp.202000269>
 19. Jakobovits A, Amado RG, Yang X, Roskos L, Schwab G (2007) From XenoMouse technology to panitumumab, the first fully human antibody product from transgenic mice. *Nat Biotechnol* 25:1134–1143. <https://doi.org/10.1038/nbt1337>
 20. Okada R, Maruoka Y, Furusawa A, Inagaki F, Nagaya T, Fujimura D, Choyke PL, Kobayashi H (2019) The effect of antibody fragments on CD25 targeted regulatory T cell near-infrared photoimmunotherapy. *Bioconjug Chem* 30:2624–2633. <https://doi.org/10.1021/acs.bioconjchem.9b00547>
 21. Sato K, Sato N, Xu B, Nakamura Y, Nagaya T, Choyke PL, Hasegawa Y, Kobayashi H (2016) Spatially selective depletion of tumor-associated regulatory T cells with near-infrared photoimmunotherapy. *Sci Transl Med* 8:352ra110. <https://doi.org/10.1126/scitranslmed.aaf6843>
 22. Kato T, Okada R, Furusawa A et al (2021) Simultaneously combined cancer cell- and CTLA4-targeted NIR-PIT causes a synergistic treatment effect in syngeneic mouse models. *Mol Cancer Ther*. <https://doi.org/10.1158/1535-7163.Mct-21-0470>
 23. Hoffman RM (1999) Orthotopic metastatic mouse models for anticancer drug discovery and evaluation: a bridge to the clinic. *Invest New Drugs* 17:343–359. <https://doi.org/10.1023/a:1006326203858>
 24. Hoffman RM (2015) Patient-derived orthotopic xenografts: better mimic of metastasis than subcutaneous xenografts. *Nat Rev Cancer* 15:451–452. <https://doi.org/10.1038/nrc3972>

Publisher's Note Springer Nature remains neutral with regard to jurisdictional claims in published maps and institutional affiliations.